Progress in NUCLEAR SCIENCE and TECHNOLOGY, Vol. 2, pp.78-84 (2011)

ARTICLE

Kinetic Integrated Modeling of Plasma Heating in Tokamaks

Hideo NUGA* and Atsushi FUKUYAMA

Department of Nuclear Engineering, Kyoto University, Kyoto 606-8501, Japan

Plasma heating and current drive can cause deformation of the momentum distribution function of the heated species. The deformation affects the heating, the loss mechanism, and the radial transport of energetic ions. The fusion reaction rate and the propagation of RF electric fields is also influenced by the deformation. Therefore, self-consistent heating analysis including the deformation of the distribution function is required for quantitative analysis. In the present analysis, the deformation of the distribution function and the behavior of radial diffusion during heating in tokamak plasmas are studied using the integrated tokamak modeling code TASK and its components TASK/FP and TASK/WM. The newly extended bounce averaged Fokker-Planck component TASK/FP implements relativistic and energy conservative collision models, and it enables us to solve the Fokker-Planck equation for each species simultaneously. Using the integrated code TASK, multi-species plasma heating is analyzed, and the effect of various radial diffusion models are examined.

KEYWORDS: Fokker-Planck, tokamak, integrated code, multi-species, self-consistent, kinetic transport

I. Introduction

In order to achieve steady thermonuclear reaction, it is necessary to heat a confined high density plasma to a high temperature. Various heating schemes, such as RF waves, neutral beam, ohmic current, and fusion reaction, have been used in magnetically confined plasmas. These plasma heating and current drive methods deform the momentum distribution function of the heated species. The deformation of the momentum distribution functions from Maxwellian affects physical phenomena such as transport, wave propagation and absorption, fusion reaction rate, and collisional relaxation processes. Since these kinetic effects can not be described by the conventional fluid model, kinetic analysis which includes the effects of deformation of the momentum distribution functions is required for a quantitative description of heating and current drive.

A number of Fokker-Planck codes have been developed[1–6] for this reason. Some of them consists of a two dimensional momentum space, multi-species, relativistic, and bounce averaged Fokker-Planck equation solver running on a radial array of non-circular flux surface. Our Fokker-Planck component, TASK/FP,[2,7] is one of them. TASK/FP has the following additional features: Firstly, it includes the non-linear collision term to second order in Legendre polynomials in order to conserve total density, momentum and energy through collision. Secondly, it calculates the momentum distribution function of each species simultaneously. Thus, the effects of collisions with the deformed distribution function of background particles are taken into account. Thirdly, it is able to couple with the full wave analysis component TASK/WM[8] in order to evaluate ICRF wave-particle interaction. Fourthly, it implements a radial diffusion term which has some momentum dependence.

The integrated tokamak modeling code, TASK, is composed of several components. The full wave component, TASK/WM,[8] calculates the wave electric field by solving Maxwell's equations including the plasma dielectric tensor. The bounce-averaged Fokker-Planck component, TASK/FP, analyzes the time evolution of the momentum distribution functions for electrons and ions by solving the Fokker-Planck equation including the quasi-linear diffusion terms calculated from the wave electric field. The dielectric tensor component, TASK/DP, calculates the plasma dielectric tensor by numerically integrating the momentum distribution functions. By repeating this cycle, we can describe the time evolution or the steady state of the wave heating and current drive.

We analyze multi-species heating of a plasma composed of four particle species: electron, deuteron, triton and α particle. For the cases we studied, neutral beam injection, ICRF wave, and 3.5 MeV α particles which are generated by nuclear reaction are used as heat sources. The ICRF waves generate energetic ions at the fundamental and higher harmonic cyclotron resonance; a high-energy tail of the momentum distribution function, which affects the absorption of the ICRF waves, is formed. In the case of the second cyclotron harmonic, a small fraction of ions is strongly accelerated and a stronger energetic tail is generated. Neutral beam and fusion reaction sources lead to non-Maxwell distribution functions, and these distribution functions affect the other species through collisions. In the present analysis, we have introduce two radial diffusion models: one is the diffusion coefficient without momentum dependence, and the other depends on momentum.

In Section II, the physics model and the features of TASK/FP are explained. In Section III, numerical results of

*Corresponding author, E-mail:nuga@p-grp.nucleng.kyoto-u.ac.jp

multi-species heating analysis in ITER plasmas are shown using the integrated code TASK. The last section is devoted to conclusions.

II. Fokker-Planck Component TASK/FP

First, we describe the Fokker-Planck component, TASK/FP, which solves the bounce averaged Fokker-Planck equation:

$$\frac{\partial f_s}{\partial t} = C(f_s) + Q(f_s) + D(f_s) + L(f_s) + S \qquad (1)$$

where the terms $C,\ Q,\ D,\ L,$ and S denote collision due to Coulomb collision, quasi-linear diffusion due to wave-particle interaction, radial transport, loss, and source, respectively. f_s denotes the momentum distribution function for species s, $f_s(p, \theta, \rho, t)$, where p and θ are the momentum and pitch angle at the minimum magnetic field point on the magnetic surface and ρ is the normalized minor radius of the magnetic surface. The pitch angle can be represented in terms of the parallel and perpendicular momentum as $\tan\theta = p_\parallel/p_\perp$. In the present analysis, we assume zero banana width limit and employ the normalized minor radius, ρ, instead of the normalized canonical angular momentum. This component can calculate the time evolution of distribution functions not only for the mainly heated species but also for other species.

1. Collision Term

Several models for the Coulomb collision are available in TASK/FP. The linear collision model[9] assumes a Maxwellian distribution for field particles. It doesn't conserve the total momentum or energy and is not adequate when various heating processes occur simultaneously. In the non-linear collision model,[9–11] the distribution functions of each field particle species, including f_s itself, are expanded in terms of Legendre polynomials, $P_l(\cos\theta)$:

$$f_s(p_s, \theta_s, \rho, t) = \sum_{l=0}^{L} f_s^{(l)}(p_s, \rho, t) P_l(\cos\theta_s) \qquad (2)$$

where θ is the pitch angle at the minimum magnetic field point on the magnetic surface. By integrating over momentum, we can calculate the non-linear collision terms. If we keep only the lowest order term ($L = 0$), the non-linear term conserves only the number of particles. Depending on the number of terms, the non-linear Coulomb collision model satisfies momentum ($L \geq 1$) and energy ($L \geq 2$) conservation. Relativistic effects are also included according to the formulation by Braams.[11]

In the case of Maxwellian momentum distribution function, the collision operator has no poloidal angle dependence, since the density and temperature are uniform on the magnetic surface. In the non-Maxwellian case, however, the poloidal angle dependence generally appears. In the present analysis, the bounce averaged non-linear collision operator is evaluated by the momentum distribution function at the poloidal angle of minimum magnetic field strength and its poloidal angle dependence is assumed to be weak.

2. Radial Transport Term

The radial transport term $D(f_s)$ is composed of radial diffusion and pinch terms. In the present analysis, two diffusion model are employed, one is constant in momentum space and the other depends on momentum as:

$$D_\rho \propto \frac{\bar{D}(\rho)}{\sqrt{1 + p^2/p_{th}^2(\rho)}} \qquad (3)$$

where $p_{th}(\rho)$ denote the thermal momentum at the normalized minor radius ρ. The latter model simulates the finite gyroradius effect due to turbulence with $k_\perp r_{\mathrm{g,th}} \sim 1$ where $k_\perp$ is the typical perpendicular wave number and $r_{\mathrm{g,th}}$ is the thermal gyroradius. The spatial diffusion across a magnetic field can be expressed as:[12]

$$D_\perp \propto \sum_{\boldsymbol{k}} \sum_n \int_{-\infty}^{\infty} d\omega \left[|E^2(\boldsymbol{k}, \omega)| \times \frac{k_\perp^2}{k^2} J_n^2(\zeta_1) \delta(n\Omega + k_\parallel v_\parallel - \omega) \right], \qquad (4)$$

where $|E^2(\boldsymbol{k}, \omega)|$ denotes the fluctuation spectrum and $J_n(\zeta)$ is the Bessel function of the nth order with the argument $\zeta = k_\perp v_\perp/\Omega = k_\perp r_g$. $\boldsymbol{k}$ and ω are the wave vector and the frequency of the fluctuation. The quasi-linear theory has shown that the radial diffusion coefficient in a magnetized plasma is proportional to $J_n^2(\zeta)$ or similar terms. Since the gyro radius r_g of energetic ion is much larger than $r_{\mathrm{g,th}}$ and $k_\perp$ spectrum of the turbulence is usually broad, $J_n^2(\zeta)$ dependence may be approximated by $1/\zeta$ by the use of the asymptotic form, $J_n(\zeta) \propto 1/\sqrt{\zeta}$. Therefore, from Eq. (4), we conclude that the radial diffusion scales as $1/\sqrt{p_\perp^2}$. For simplicity, $p_\perp$ in the dependence is replaced by p in our calculations.

The radial variation of $\bar{D}$ is taken to be parabolic:

$$\bar{D}(\rho) = \bar{D}(0) + (\bar{D}(1) - \bar{D}(0))\rho^2 \qquad (5)$$

This is because the radial diffusion coefficient observed in typical experiments is tend to be weak in the plasma core region while it is typically strong at the plasma edge region.

The pinch effect which sustains the density profile was introduced through the radial friction coefficient F_r, which satisfies

$$\int d\boldsymbol{p} \left(D_\rho \frac{\partial f}{\partial \rho} - F_\rho f \right) = 0. \qquad (6)$$

Since we have assumed the zero banana width limit, the neoclassical radial transport is neglected because it is assumed that the anomalous transport due to turbulence is sufficiently large compared to the neoclassical transport.

3. Source Term

The source term $S(f_s)$ includes particle sources such as NBI and α particles generated by fusion reaction. The neutral beam is a source of accelerated ions and electrons which have the same velocity. In TASK/FP, the deposition profile is constant in time and the pitch angle of the beam is constant in the radial direction. The radial deposition profile is approximated

by a Gaussian distribution. The fusion reaction rates $\mathcal{R}_{**}$ for D-D, D-T, and T-T reactions are calculated in TASK/FP. Since the reaction rate depends on the momentum distribution function of the fuel ions, it is calculated using[13)]

$$\mathcal{R}_{ab} = \iint \sigma_T(E_b) v' f_a(p_a, \theta_a, \rho, t) f_b(p_b, \theta_b, \rho, t) d\boldsymbol{p}_a d\boldsymbol{p}_b \quad (7)$$

where v', E_b, and σ_T denote the relative velocity between reacting ions, the kinetic energy of species b, and the cross section of fusion reaction, respectively.

4. Numerical Method

In TASK/FP, the full implicit method is used for time advancing. The difference equation for time advancing is

$$\frac{\boldsymbol{f}_s^{t+1} - \boldsymbol{f}_s^t}{\Delta t} = \boldsymbol{A}_s^{t+1} \boldsymbol{f}_s^{t+1} + \boldsymbol{H}_s, \quad (8)$$

where $\boldsymbol{A}_s^t$ and $\boldsymbol{H}_s$ denote the coefficient matrix and the source term vector at time step t for species s. The equation is rewritten as:

$$\boldsymbol{f}_s^{t+1} = \left(\boldsymbol{I} - \boldsymbol{A}_s^{t+1} \Delta t\right)^{-1} \left(\boldsymbol{f}_s^t + \boldsymbol{H}_s \Delta t\right) \quad (9)$$

Since $\boldsymbol{A}_s^{t+1}$ in the right-hand side of Eq. (9) depends on $\boldsymbol{f}_s^{t+1}$, iteration is needed until $\boldsymbol{f}_s^{t+1}$ converges.

In the following calculation, the time step Δt has same value for all species. The value of Δt is continually adjusted to make the iterative scheme converge as quickly as possible. The value always satisfies: $1\mathrm{ms} < \Delta t < 30\mathrm{ms}$. When the deformation of the momentum distribution function is large, the value of Δt tends to be small and *vice versa*.

5. Parallel Processing

TASK/FP is parallelized using the parallel matrix solver PETSc[14)] in order to reduce the calculation time. The calculation is split into several processes, the number of which is a divisor of the number of radial grid points. The reduction of computation time through parallel processing is shown in **Fig. 1**.

Using a cluster computer with 128 cores on 16 nodes, a test calculation is done using various numbers of nodes and cores. The test calculation describes temperature relaxation among electron and ions without radial diffusion using 64 grid points. Figure 1 shows the calculation time (user time and system time) vs. the number of grid points per node for various numbers of cores. It is found that the user time (blue lines) is almost inversely proportional to the number of cores but is nearly independent of numbers of grid points per node. On the other hand, the system time (red lines) depends on not only the number of cores, but also on numbers of grid points per node. The system time increases as numbers of grids per node increases.

From these results, it is found that the calculation time decreases as numbers of cores increases and numbers of grid points per node decreases in our calculation environment.

III. Numerical Results of Multi Species Heating

We carried out numerical analysis of multi species heating with two radial diffusion models. The first diffusion model

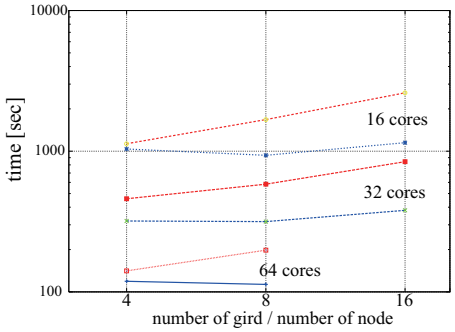

Fig. 1 The user time (blue lines) and the system times (red lines) for different numbers of cores. The horizontal axis denotes the number of radial grids per a node and the vertical axis denotes the calculation time. For example, the lowest (blue) and second lowest lines (red) denote the calculation time of the test calculation using 64 cores.

Table 1 Plasma parameters

major radius	R_0	6.2 m
minor radius	a	2.0 m
elongation	κ	1.7
triangularity	δ	0.33
magnetic field on axis	B_0	5.3 T
initial temperature on axis	T_0	10.0 keV
initial temperature on surface	T_s	1.0 keV
initial density on axis	n_0	$1{\times}10^{20}/\mathrm{m}^3$
initial density on surface	n_s	$1\times10^{19}/\mathrm{m}^3$
initial deuterium ratio	n_D/n_e	0.5
tritium ratio	n_T/n_e	0.5
NBI energy	E_{NBI}	1 MeV
α particle energy	E_α	3.5 MeV
ICRF wave frequency	f_{RF}	55.0 MHz

is parabolic in the radial direction ($\bar{D}(\rho = 0) = 0.1\mathrm{m/s}^2$, $\bar{D}(\rho = 1) = 1.0\mathrm{m/s}^2$) and constant in momentum space. The second model is also parabolic in radial direction but depends on the momentum as Eq. (3). In these analyses, we used the parameters in **Table 1**, simulating ITER like tokamaks. We used a 55 MHz ICRF wave, 1 MeV deuterium NBI, and 3.5 MeV α particles as heat sources. The α particle generation rate is calculated by numerical integration [Eq. (7)]. Electrons and fast tritons accelerated by ICRF, fast deuterium injected by NBI, and fast α particles generated by fusion reaction collide with each other and transfer their energy through collision. **Figure 2** shows wave absorption profiles calculated by TASK/WM. The tritons absorb wave power near the second harmonic resonance surface as shown in Fig. 2(a). In the following TASK/FP calculation, the input ICRF wave amplitude is held constant.

1. Case without Momentum Dependence

First, we studied the effect of radial transport without momentum dependence. In this analysis, the NBI power was 31.7 MW, the α particle heating power was $16.6 \sim 23.4$ MW,

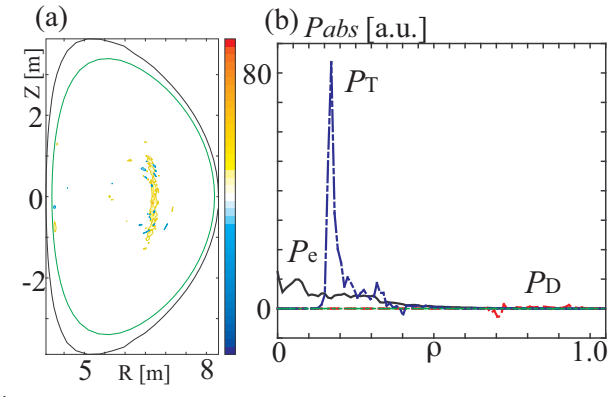

Fig. 2 ICRF wave absorption profiles. (a) Absorbed power density profile for T on poloidal cross section. (b) Radial profile of absorbed power density $P_{\rm abs}$.

and the initial value of the ICRF heating power was 14.2 MW (6.81 MW for electrons and 7.39 MW for triton). The absorption power increases to 16.9 MW. Since the input wave amplitude is fixed in this calculation, the absorbed power increases due to the generation of fast ions. **Figure 3** shows the contours of distribution functions for electrons, deuterons, tritons, and α particles at 1 sec after the onset of heating. Anisotropy of the deuteron and triton distribution functions (Figs. 3(b) and (c)) is due to NBI and ICRF wave absorption. Cyclotron harmonic resonance mainly increases the perpendicular momentum of particles. There are two tips in Fig. 3(c) because of trapped particle effects. Figure 3(d) shows that the distribution function of He has a peak at 3.5 MeV ($\bar{p} \sim 27$) . From Figs. 3(a) and 3(c), it was found that the deformation of the electron distribution function is much less than that of triton. This is because the collisional relaxation time of electrons is much shorter than that of triton.

Figure 4 shows the radial profiles of power absorption, collisional power transfer, power loss due to radial diffusion, and the sum of these terms, ΔW. From Figs. 4(a) and (b), the dominant heat mechanism for each species is confirmed. Deuteron and triton are mostly heated by external heating: NBI and ICRF. Meanwhile, electrons are heated through collision with fast α particles generated by fusion reaction and fast ions. From Figs. 4(a) and (c), we find that the diffusive power transfer profile is comparable to the power absorption profile. The reason is that, since the radial diffusion coefficient is independent of momentum space, radial diffusive power transfer increases with the increase of the population of fast ions. In Fig. 4(e), bulk temperature is estimated by the following equation around thermal momentum;

$$T_{\mathrm{bulk},s} = -\frac{p_s f_s}{\gamma_s}\left(\frac{\partial f_s}{\partial p}\right)^{-1}. \qquad (10)$$

Since the distribution function of deuterons has a strong anisotropy as is shown in Fig. 3(b), there is a large difference between averaged energy density and bulk temperature.

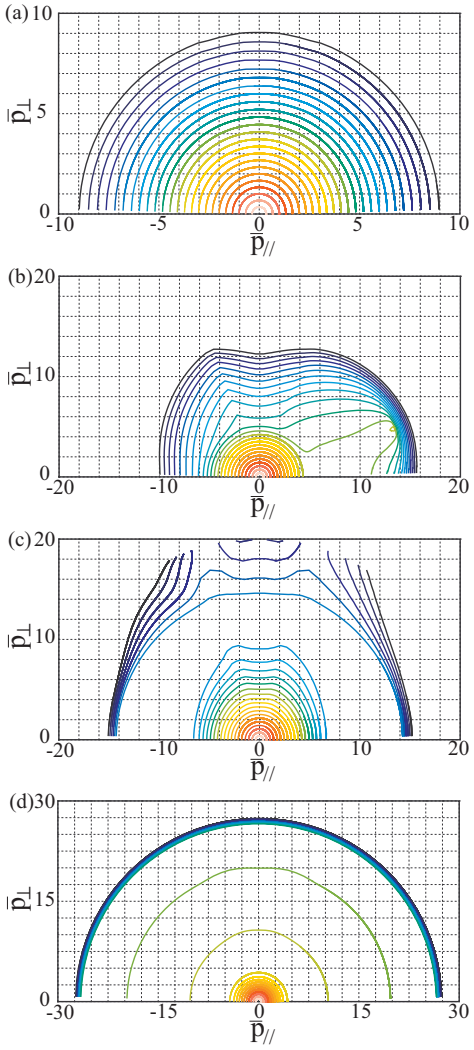

Fig. 3 Contours of distribution functions at the peak of wave absorption ($\rho = 0.17$) in 2D momentum space. (a) electron, (b) D, (c) T, (d) He. Vertical and horizontal axes are perpendicular and parallel normalized momentum. $\bar{p} \sim 15$ correspond to 1 MeV. The contours have been chosen such that they are evenly spaced when the distribution functions are Maxwellian.

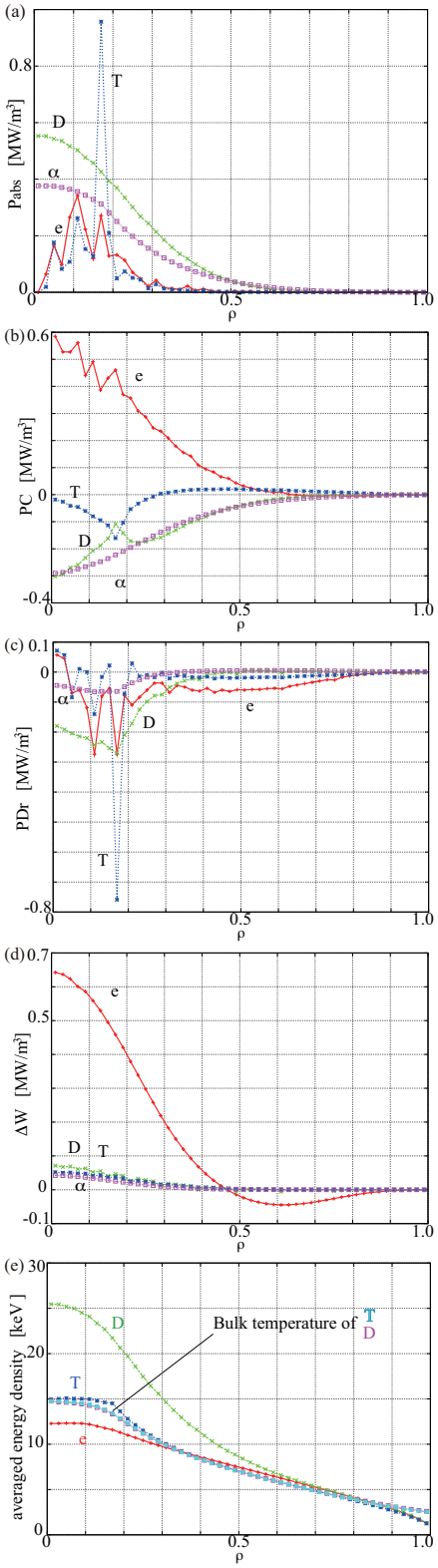

Fig. 4 Radial profile of (a) power absorbed from heat sources $P_{\rm abs}$, (b) collisional power transfer to each species P_c, (c) radial diffusion loss of power P_{D_ρ}, (d) total input power ΔW, and (e) averaged energy density $\bar{T}$. The various lines indicate electrons (red), deuterons (green), tritons (blue), and α particles (purple).

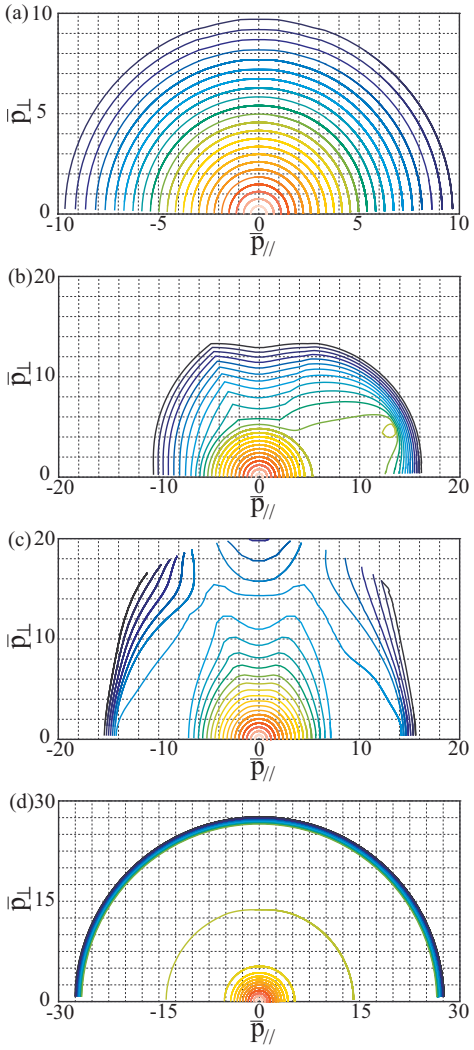

Fig. 5 Contours of distribution functions at the peak of wave absorption ($\rho = 0.17$) in 2D momentum space for the case of radial diffusion reduced for fast ions. (a) electron, (b) D, (c) T, (d) He.

2. Case with Momentum Dependence

Next, the case with radial diffusion depending on momentum is examined using the same heating source as in the previous subsection; the α particle heating power is $16.6 \sim 32.7$ MW, and the the ICRF heating power was $14.2 \sim 20.5$ MW. **Figure 5** shows contours of the distribution function for each species. Because of the momentum dependence of D_ρ, Eq. (3), the radial diffusion of fast particles is much less in this case. Therefore, the deformation of the distribution function is stronger than that of the previous case.

Figure 6 illustrates the radial profiles in this case. Since the fast particles are less diffusive, the α particle generation profile has a peak at the peak of wave absorption in Fig. 6(a). Therefore, the profile of radial diffusion loss of electron which is mainly heated by collision with α particles in Figs. 6(b), (d), and (e), are also changed.

Figure 7 shows the contour of the triton distribution function in momentum space at $\rho = 0.57$. Figure 7(a) illustrates

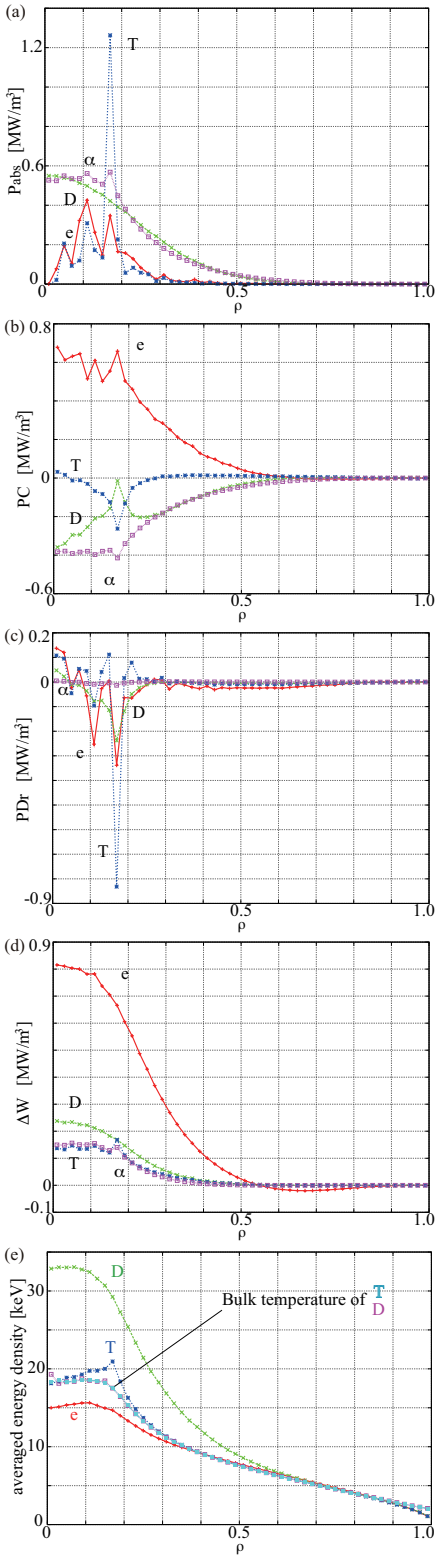

Fig. 6 Radial profile of (a) power absorbed from heat sources $P_{\rm abs}$, (b) collisional power transfer to each species P_c, (c) radial diffusion loss of power P_{D_ρ}, (d) total input power ΔW, and (e) averaged energy density $\tilde{T}$.

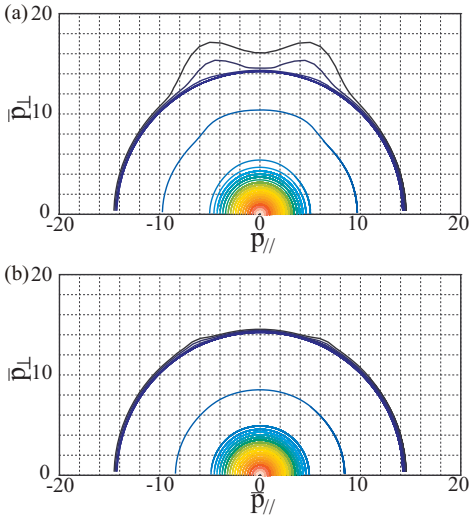

Fig. 7 Contours of the triton distribution functions at $\rho = 0.57$ in 2D momentum space. (a) D_ρ independent of $\bar{p}$, (b) D_ρ depending on $\bar{p}$

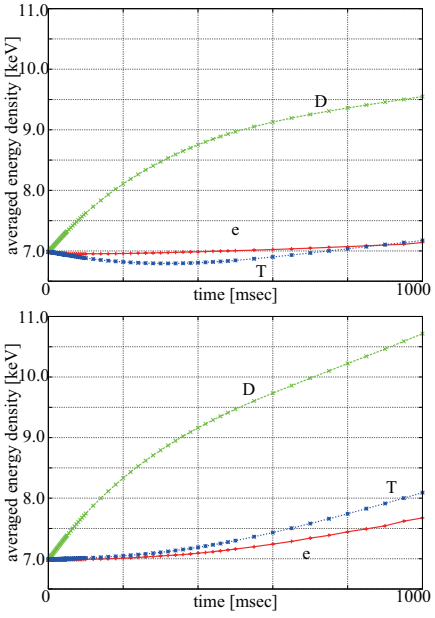

Fig. 8 Time evolution of volume averaged energy density. (a) D_ρ independent of $\bar{p}$, (b) D_ρ dependent on $\bar{p}$

the result without momentum dependence and Figure 7(b) illustrates the result with reduction for fast ions. The semicircle of these figures around $\bar{p} \sim 15$ indicates the T source due to D-D reaction, which has an energy of 1.01 MeV ($\bar{p} \sim 15$). From Fig. 7, we found that radial transport of fast ions is strongly reduced when D_ρ depends on $\bar{p}$. **Figure 8** shows the time evolution of the volume averaged energy density in the two cases. As the fast particle transport decreases, the volume averaged energy density increases.

IV. Discussion

In the present status of TASK/FP, the zero banana width approximation is used. However, it is invalid for the analysis of the fast particles. This is because the radial excursion of the orbit across a magnetic surface is rather large for high energy particles. Due to the inclusion of the finite orbit width effect, the radial profile of the density of accelerated energetic ions will be broadened, and the radial profile of the collisional power transfer in actual plasma should be broader that of the present analysis. Therefore, more accurate analysis for fast ions requires the inclusion of finite orbit width effects with the transition of particle orbits.

V. Conclusion

We have updated the Fokker-Planck component of TASK, TASK/FP, for kinetic analysis of heating and transport. The present study describes the simultaneous analysis of the time evolution of the momentum distribution functions for a multi-species plasma with radial transport. We have confirmed that plasma heating depends on the loss mechanism. More realistic radial transport models, as used in conventional one-dimensional diffusive transport simulation, and finite orbit width effects are essential for quantitative comparison with experimental observation. The implementation is underway.

Acknowledgment

The authors would like to thank Daniel L. Raburn for help in improving English in the manuscript. This work was supported in part by the Grant-in-Aid for scientific research, No. 20226017, from Japan Society for the Promotion of Science.

References

1) G. D. Kerbel, M. G. McCoy, *Phys. Fluid*, **28**, 3629, (1985).
2) A. Fukuyama, T. Ueeda, *Proc. 17th euro. conf.*, Amsterdam, (1990).
3) G. Giruzzi, I. Findone, X. Garbet, *Nucl. Fusion*, **32**, 1011, (1992).
4) J. S. McKenzie, M. R. O'Brien, M. Cox, *Comput. Phys. Comm.*, **66**, 194, (1991).
5) R. W. Harvey, M. G. McCoy, *Proceedings of the IAEA Technical Committee Meeting on Simulation and Modeling of Thermonuclear Plasmas*, Montreal, Canada, 1992, (USDOC NTIS Document No. DE93002962).
6) R. W. Harvey, M. G. McCoy, *The CQL3D Fokker-Planck Code*, http://www.compxco.com/cql3d.html (2005).
7) H. Nuga and A. Fukuyama, *J. Plasma Fusion Res.*, **8**, 1125, (2009).
8) A. Fukuyama *et al.*, *Proc. of 20th IAEA FEC*, (Villamoura, Portugal, 2004), IAEA-CSP-25/CD/TH/P2-3.
9) C. F. F. Karney, *Comput. Phys. Rep.*, **4**, 183-244, (1986).
10) J. Killeen, G. D. Kerbel, M. G. McCoy, A. A. Mirin, *Computational Methods for Kinetic Models of Magnetically Confined Plasmas*, Springer-Verlag, New York, (1986).
11) B. J. Braams, C. F. F. Karney, *Phys. Fluid*, **B1**, 1355-1368, (1989).
12) S. Ichimaru, *Basic principles of plasma physics: a statistical approach*, Westview Press, (1973).
13) J. D. Huba, *NRL PLASMA FORMULARY*, The Office of Naval Research, Washington DC, (2007).
14) S. Balay *et al.*, *PETSc Users Manual*, http://www.mcs.anl.gov/petsc/petsc-as/snapshots/petsc-3.0.0/docs/manual.pdf (2008).